mathematics

MDPI

Article

Approximate Closed-Form Solutions for the Maxwell-Bloch Equations via the Optimal Homotopy Asymptotic Method

Remus-Daniel Ene [1,†], Nicolina Pop [2,*,†], Marioara Lapadat [1,†] and Luisa Dungan [3,†]

[1] Department of Mathematics, Politehnica University of Timisoara, 2 Victoria Square, 300006 Timisoara, Romania
[2] Department of Physical Foundations of Engineering, Politehnica University of Timisoara, 2 Vasile Parvan Blvd., 300223 Timisoara, Romania
[3] Mech Machines Equipment & Transports Department, Politehnica University of Timisoara, 300222 Timisoara, Romania
* Correspondence: nicolina.pop@upt.ro
† These authors contributed equally to this work.

Abstract: This paper emphasizes some geometrical properties of the Maxwell–Bloch equations. Based on these properties, the closed-form solutions of their equations are established. Thus, the Maxwell–Bloch equations are reduced to a nonlinear differential equation depending on an auxiliary unknown function. The approximate analytical solutions were built using the optimal homotopy asymptotic method (OHAM). These represent the ε-approximate OHAM solutions. A good agreement between the analytical and corresponding numerical results was found. The accuracy of the obtained results is validated through the representative figures. This procedure is suitable to be applied for dynamical systems with certain geometrical properties.

Keywords: Maxwell–Bloch equations; Hamilton–Poisson realization; periodical orbits; symmetries; optimal homotopy asymptotic method

MSC: 65L60; 76A10; 76D05; 76D10; 76M55

check for updates

Citation: Ene, R.-D.; Pop, N.; Lapadat, M.; Dungan, L. Approximate Closed-Form Solutions for the Maxwell-Bloch Equations via the Optimal Homotopy Asymptotic Method. *Mathematics* **2022**, *10*, 4118. https://doi.org/10.3390/math10214118

Academic Editor: Maria C. Mariani

Received: 13 October 2022
Accepted: 2 November 2022
Published: 4 November 2022

1. Introduction

In the last period, the dynamical systems were studied related to their important applications in electrical engineering, medicine and economics, such as complete synchronization or optimization of nonlinear system performance, secure communications, and so on. The stabilization of the T system via linear controls was explored in [1]. The Rikitake two-disk dynamo system was studied by [2] and applied in [3,4]. Other geometrical properties of the dynamical systems, such as the Hamiltonian realization, the equilibria points, and integrable deformations, were analyzed in [5–19].

The interaction between laser light and a material sample composed of two-level atoms is described by Maxwell equations of the electric field and by Schrödinger equations for the probability amplitudes of the atomic levels. The Maxwell–Bloch equations were obtained by coupling the Maxwell equations with the Bloch equation, and their important geometrical properties were explored in [20–30], and so on.

An important geometrical property of a dynamical system is the existence of symmetries. The system considered here admits a symmetry with respect to the Oz-axis.

The paper is organized as follows: Section 2 provides a brief description of the geometrical properties and the closed-form solutions of the Maxwell–Bloch system. The next section emphasizes the OHAM method. The ε-approximate solutions are built in Section 4 using the OHAM technique. The corresponding numerical results and the presented solutions are discussed in Section 5. The relevance of the method is highlighted in Tables and Figures. The last section of this work is dedicated to the conclusions.

2. The Maxwell–Bloch Equations

2.1. Hamilton–Poisson Realization

The real-valued Maxwell–Bloch equations are (see [11,23,24,31]):

$$\begin{cases} \dot{x} = y \\ \dot{y} = x \cdot z \\ \dot{z} = -x \cdot y \end{cases} , \tag{1}$$

where the unknown functions x, y and z depend on $t > 0$, and the dot symbol denotes a derivative with respect to t.

In this section, we also recall [31] some geometrical properties of the system (1).

The considered system has a Hamilton–Poisson realization with the Hamiltonian $H(x, y, z) = \frac{1}{2}(y^2 + z^2)$ and a Casimir given by $C(x, y, z) = z + \frac{1}{2}x^2$.

Remark 1. *For the initial conditions*

$$x(0) = x_0 \ , \quad y(0) = y_0 \ , \quad z(0) = z_0 \ , \tag{2}$$

the phase curves of dynamics (1) *are the intersections of the surfaces* $\frac{1}{2}(y^2 + z^2) = \frac{1}{2}(y_0^2 + z_0^2)$ *and* $z + \frac{1}{2}x^2 = z_0 + \frac{1}{2}x_0^2$.

2.2. Closed-Form Solutions

Using the results presented in Section 2.1, in the present section, the closed-form solutions of the system Equation (1) are built.

For an unknown smooth function $v(t)$, by performing the transformations:

$$\begin{cases} y = R \cdot \sqrt{2} \cdot \sin(v(t)) \\ z = R \cdot \sqrt{2} \cdot \cos(v(t)) \end{cases} , \quad R = \sqrt{\frac{1}{2} \cdot (y_0^2 + z_0^2)} \ , \tag{3}$$

the second equation from Equation (1) becomes:

$$x = \dot{v}(t). \tag{4}$$

First equation from Equation (1) yields to:

$$\ddot{v}(t) - R \cdot \sqrt{2} \cdot \sin(v(t)) = 0 \ . \tag{5}$$

The initial conditions $v(0)$ and $\dot{v}(0)$ are obtained from Equations (2), (3) and (4):

$$v(0) = \arctan \frac{y_0}{z_0} \ , \quad \dot{v}(0) = x_0, \quad \text{for} \ \ z_0 \neq 0 \ . \tag{6}$$

Remark 2. *Equations (3) and (4) give a closed-form solution of the system Equation (1).*

In the last decades, there have been several analytical methods for solving the nonlinear differential problem given by Equations (5) and (6), such as the function method [32], the multiple scales technique [33], the optimal homotopy perturbation method (OHPM) [34,35], the least squares differential quadrature method [36], the polynomial least squares method [37], the optimal iteration parametrization method (OIPM) [38], the optimal homotopy asymptotic method (OHAM) [39], the homotopy analysis method (HAM) and the homotopy perturbation method (HPM) [40], the variational iteration method (VIM) [41], the optimal variational iteration method (OVIM) [42], the Fourier spectral method [43], and the piecewise reproducing kernel method [44].

The nonlinear differential problem given by Equations (5) and (6) is analytically solved using the optimal homotopy asymptotic method (OHAM).

3. Basic Ideas of the OHAM Technique

In this section, we recall some mathematical tools to explain the approximate analytic solution obtained via the OHAM technique.

Firstly, the general form for the nonlinear differential equation is chosen as [45]:

$$\mathcal{L}\Big(F(t)\Big) + \mathcal{N}\Big(F(t)\Big) = 0, \tag{7}$$

with the initial conditions

$$\mathcal{B}\Big(F(t), \frac{dF(t)}{dt}\Big) = 0, \tag{8}$$

where $\mathcal{L}$ is an arbitrary linear operator, $\mathcal{N}$ is the corresponding nonlinear operator, $\mathcal{B}$ is an operator characterizing the boundary conditions, and $F(t)$ is the unknown smooth function.

Let $\tilde{F}(t)$ be the approximate solution of Equation (7). The error obtained by replacing the exact solution $F(t)$ of Equation (7) with the approximate ones $\tilde{F}(t)$ is given by the remainder:

$$\mathcal{R}(t,\tilde{F}) = \mathcal{L}\Big(\tilde{F}(t)\Big) + \mathcal{N}\Big(\tilde{F}(t)\Big), \;\; t > 0\,. \tag{9}$$

If $p \in [0,\ 1]$ is an embedding parameter, then the homotopic relation is given by:

$$\begin{aligned} &\mathcal{H}\Big[\mathcal{L}\Big(\Phi(t,p)\Big),\ H(t,C_i),\ \mathcal{N}\Big(\Phi(t,p)\Big)\Big] = \\ &= \mathcal{L}\Big(F_0(t)\Big) + p\Big[\mathcal{L}\Big(F_1(t,C_i)\Big) - H(t,C_i)\mathcal{N}\Big(F_0(t)\Big)\Big] = 0, \end{aligned} \tag{10}$$

where $H(t,C_i) \neq 0$ is an auxiliary convergence-control function depending on the variable t and the unknown parameters $C_1, C_2, \ldots, C_s$.

When p increases from 0 to 1, the solution $\Phi(t,p)$ of Equation (7) varies from $\Phi(t,0) = F_0(t)$ to the solution $\Phi(t,1) = F(t)$ of Equation (7).

If we consider the unknown function $\Phi(t,p)$ in the form:

$$\Phi(t,p) = F_0(t) + pF_1(t,C_i), \tag{11}$$

and equate the coefficients of p^0 and p^1, respectively, the deformations problems are obtained.

These are called:

- The zeroth-order deformation problem

$$\mathcal{L}\Big(F_0(t)\Big) = 0, \quad \mathcal{B}\Big(F_0(t), \frac{dF_0(t)}{dt}\Big) = 0, \tag{12}$$

- The first-order deformation problem

$$\begin{aligned} &\mathcal{L}\Big(F_1(t,C_i)\Big) = H(t,C_i)\mathcal{N}\Big(F_0(t)\Big), \\ &\mathcal{B}\Big(F_1(t,C_i), \tfrac{dF_1(t,C_i)}{dt}\Big) = 0, \;\; i = 1,2,\ldots,s. \end{aligned} \tag{13}$$

By solving the linear Equation (12), the initial approximation can be obtained.

In order to compute $F_1(t,C_i)$ from Equation (13), the nonlinear operator $\mathcal{N}$ is considered to have the general form:

$$\mathcal{N}(F_0(t)) = \textstyle\sum_{i=1}^{n} h_i(t)g_i(t), \tag{14}$$

where n is a positive integer, and $h_i(t)$ and $g_i(t)$ are known functions that depend on $F_0(t)$ and $\mathcal{N}$.

For $m = 1, 2, ,\cdots$ let us consider the set S_m containing the functions

$$h_1, h_2, \cdots, h_m , \tag{15}$$

chosen as linearly independent functions in the vector space of the continuous differentiable functions on the interval $I = (0, \infty)$, such that $S_{m-1} \subseteq S_m$.

Following the procedure described in [45], the computation function $F_1(t, C_i)$ has the form:

$$F_1(t, C_i) = \textstyle\sum_{i=1}^{m} H_i(t, h_j(t), C_j) g_i(t), \quad j = 1, \ldots, s, \tag{16}$$

or

$$\begin{aligned} &F_1(t, C_i) = \textstyle\sum_{i=1}^{m} H_i(t, g_j(t), C_j) h_i(t), \quad j = 1, \ldots, s, \\ &\mathcal{B}\Big(F_1(t, C_i), \tfrac{dF_1(t,C_i)}{dt}\Big) = 0, \end{aligned} \tag{17}$$

where $H_i(t, h_j(t), C_j)$ represents a linear combination of the functions h_j, $j = 1, \ldots, s$ and the parameters C_j, $j = 1, \ldots, s$. The summation limit m is an arbitrary positive integer number.

For $p = 1$, the first-order analytical approximate solution of Equations (7) and (8), taking into account Equation (11), has the form:

$$\tilde{F}(t, C_i) = F(t, 1) = F_0(t) + F_1(t, C_i), \tag{18}$$

where $\tilde{F}(t, C_i)$ is a real linear combination of these functions h_j.

The unknown parameters $C_1, C_2, \ldots, C_s$ can be optimally identified by means of various methods, such as the least square method, the Kantorowich method, the collocation method, the Galerkin method, or the weighted residual method.

The first-order approximate solution (18) is well-determined if the convergence-control parameters are known.

Using the functions given by Equation (15), we recall some types of approximate solutions of Equation (7) from [46].

Definition 1. *A sequence of functions $\{s_m(t)\}_{m\geq 1}$ of the form*

$$s_m(t) = \sum_{i=1}^{m} \alpha_m^i \cdot h_i(t) , \quad m \geq 1, \ \alpha_m^i \in \mathbb{R}, \tag{19}$$

is called an OHAM sequence of the Equation (7).

Functions of the OHAM sequences are called OHAM functions of Equation (7).

The OHAM sequences $\{s_m(t)\}_{m\geq 1}$ with the property

$$\lim_{m\to\infty} \mathcal{R}(t, s_m(t)) = 0$$

are called convergent to the solution of Equation (7).

Definition 2. *The OHAM functions $\tilde{F}$ satisfying the conditions*

$$\Big|\mathcal{R}(t, \tilde{F}(t))\Big| < \varepsilon, \ \mathcal{B}\Big(\tilde{F}(t, C_i), \frac{d\tilde{F}(t, C_i)}{3t}\Big) = 0 \tag{20}$$

are called ε-approximate OHAM solutions of Equation (7).

Definition 3. *The OHAM functions $\tilde{F}$ satisfying the conditions*

$$\int_0^\infty \mathcal{R}^2(t, \tilde{F}(t))\, dt \leq \varepsilon, \;\; \mathcal{B}\left(\tilde{F}(t, C_i), \frac{d\tilde{F}(t, C_i)}{dt}\right) = 0 \tag{21}$$

are called weak ε-approximate OHAM solutions of Equation (7) of the real interval $(0, \infty)$.

Remark 3. *It is easy to see that any ε-approximate OHAM solution of Equation (7) is also a weak ε-approximate OHAM solution. It follows that the set of weak ε-approximate OHAM solutions of Equation (7) also contains the approximate OHAM solutions of Equation (7).*

The following theorem states the existence of weak ε-approximate OHAM solutions of Equation (7) and furnishes the way to construct them.

Theorem 1. *Equation (7) admits a sequence of weak ε-approximate OHAM solutions.*

Proof. The first step of the proof is to construct the OHAM sequences $\{s_m\}_{m \geq 1}$.

Let us consider the approximate OHAM solutions of the type:

$$\tilde{F}(t) = \sum_{i=1}^{n} C_m^i \cdot h_i(t)\,, \;\; \text{where} \;\; m \geq 1 \;\; \text{is fixed arbitrary.}$$

In the following, the unknown parameters C_m^i, $i \in \{1,\, 2,\, \cdots, n\}$ will be determined. Substituting the approximate solutions $\tilde{F}$ in Equation (7), one obtains the expression:

$$\mathcal{R}(t, C_m^i) := \mathcal{R}(t, \tilde{F}).$$

Attaching to Equation (7) the following real functional

$$\mathcal{J}_1(C_m^i) = \int_0^\infty \mathcal{R}^2(t, C_m^i)\, dt \tag{22}$$

and imposing the initial conditions, we can determine $l \in \mathbb{N}$, $l \leq m$, such that $C_m^1, C_m^2, \cdots, C_m^l$ are computed as $C_m^{l+1}, C_m^{l+2}, \cdots, C_m^n$.

Replacing $C_m^1, C_m^2, \cdots, C_m^l$ in Equation (22), the values of $\tilde{C}_m^{l+1}, \tilde{C}_m^{l+2}, \cdots, \tilde{C}_m^n$ are computed as the values, which give the minimum of the functional (22).

Using again the initial conditions, the values $\tilde{C}_m^1, \tilde{C}_m^2, \cdots, \tilde{C}_m^l$ as functions of $\tilde{C}_m^{l+1}, \tilde{C}_m^{l+2}, \cdots, \tilde{C}_m^n$ are determined.

Using the constants $\tilde{C}_m^1, \tilde{C}_m^2, \cdots, \tilde{C}_m^n$ thus determined, the following OHAM functions

$$s_m(t) = \sum_{i=1}^{n} \tilde{C}_m^i \cdot h_i(t) \tag{23}$$

are constructed.

The second step of the proof is to show that the above OHAM functions $s_m(t)$ are weak ε-approximate OHAM solutions of Equation (7).

Based on the way the OHAM functions $s_m(t)$ are computed and taking into account that $\bar{F}$ given by (18) are OHAM functions for Equation (7), it follows that:

$$0 \leq \int_0^\infty \mathcal{R}^2(t, s_m(t))\, dt \leq \int_0^\infty \mathcal{R}^2(t, \bar{F}(t))\, dt\,, \;\; \forall\, m \geq 1.$$

Therefore,

$$0 \le \lim_{m\to\infty} \int_0^\infty \mathcal{R}^2(t, s_m(t))\, dt \le \lim_{m\to\infty} \int_0^\infty \mathcal{R}^2(t, \tilde{F}(t))\, dt.$$

Since $\tilde{F}(t)$ is convergent to the solution of Equation (7), we obtain:

$$\lim_{m\to\infty} \int_0^\infty \mathcal{R}^2(t, s_m(t))\, dt = 0.$$

It follows that for all $\varepsilon > 0$, there exists $m_0 \ge 1$ such that for all $m \ge 1$, $m > m_0$, the sequence $s_m(t)$ is a weak ε-approximate OHAM solution of Equation (7). □

Remark 4. *The proof of the above theorem gives us a way to determine a weak ε-approximate OHAM solution of Equation (7), $\tilde{F}$. Moreover, taking into account Remark 1, if $|\mathcal{R}(t, \tilde{F})| < \varepsilon$, then $\tilde{F}$ is also an ε-approximate OHAM solution of the considered equation.*

4. Approximate Analytic Solutions via OHAM

For the unknown function v, the approximate solutions of Equation (5) with initial conditions given by Equation (6) are obtained.

The linear operator $\mathcal{L}\Big(v\Big)$ has the following expression:

$$\mathcal{L}\Big(v\Big)(t) = \ddot{v} + \omega_0^2 v, \tag{24}$$

where $\omega_0 > 0$ is an unknown parameter at this moment. Therefore, the form of the nonlinear operator $\mathcal{N}\Big(v\Big)$ corresponding to the unknown function v is obtained from Equation (5) by:

$$\mathcal{N}\Big(v\Big)(t) = -\omega_0^2 v - R\sqrt{2}\cdot \sin(v)\ . \tag{25}$$

In Equation (25), we can use the approximate expansion

$$\sin(v) \simeq \sum_{i=0}^{N_{max}} (-1)^i \cdot \frac{v^{2i+1}}{(2i+1)!}\ , \tag{26}$$

where N_{max} is an arbitrary integer number.

There are many possibilities to choose the auxiliary function $H(t, C_i)$; one of them could be

$$H(t, C_i) = C, \tag{27}$$

or

$$H(t, C_i) = C_1\ \cos(\omega_0 t) + B_1\ \sin(\omega_0 t),$$

or

$$H(t, C_i) = C_1\ \cos(\omega_0 t) + B_1\ \sin(\omega_0 t) + C_2\ \cos(3\omega_0 t) + B_2\ \sin(3\omega_0 t),$$

or

$$H(t, C_i) = C_1\ \cos(\omega_0 t) + B_1\ \sin(\omega_0 t) + C_2\ \cos(3\omega_0 t) + B_2\ \sin(3\omega_0 t) + C_3\ \cos(5\omega_0 t) + B_3\ \sin(5\omega_0 t),$$

and so on.

4.1. The Zeroth-Order Deformation Problem

For the initial approximation v_0, Equation (12) becomes:

$$\ddot{v} + \omega_0^2 v = 0,\quad v(0) = \arctan\frac{y_0}{z_0}\ ,\ \ \dot{v}(0) = x_0 \tag{28}$$

with the solution

$$v_0(t) = v(0)\ \cos(\omega_0 t) + \frac{\dot{v}(0)}{\omega_0}\ \sin(\omega_0 t). \tag{29}$$

4.2. The First-Order Deformation Problem

For the initial approximation $v_0(t)$ given by Equation (29), using Equation (26), the nonlinear operator Equation (25) becomes:

$$\begin{aligned}&\mathcal{N}(v_0)(t) = -\omega_0^2\Big(v(0)\ \cos(\omega_0 t) + \tfrac{\dot{v}(0)}{\omega_0}\ \sin(\omega_0 t)\Big) + \\ &\sum_{i=1}^{N_{max}} \frac{(-1)^i}{(2i+1)!}\cdot\Big(v(0)\ \cos(\omega_0 t) + \frac{\dot{v}(0)}{\omega_0}\ \sin(\omega_0 t)\Big)^{2i+1},\end{aligned} \tag{30}$$

and depends on the elementary functions $\cos((2k+1)\omega_0 t), \sin((2k+1)\omega_0 t), k = 1, 2, 3, \cdots$.

Hence, the OHAM sequences of the nonlinear Equation (5) have the form:

$$\{\cos((2k+1)\omega_0 t)\ ,\ \ \sin((2k+1)\omega_0 t)\}_{k\geq 1}\ .$$

For $H(t, C_i)$, choosing the expression given by Equation (27) for the first-order deformation problem given by Equation (13) by integration with the first approximation $v_1(t, D_i)$ from Equation (16) becomes:

$$v_1(t, C_i) = \sum_{k=1}^{N_{max}} C_k \cdot \cos((2k+1)\omega_0 t) + B_k \cdot \sin((2k+1)\omega_0 t), \tag{31}$$

where C_i, B_i are unknown parameters, with $\sum_{k=1}^{N_{max}} C_k \ = 0$ and $\sum_{k=1}^{N_{max}} (2k+1)\cdot B_k \ = 0$, respectively.

4.3. The First-Order Analytical Approximate Solution $\bar{v}$

From Equations (29) and (31), the first-order approximate solution given by Equation (18) is obtained:

$$\begin{aligned}&\bar{v}(t) = v_0(t) + v_1(t, C_i) = v(0)\ \cos(\omega_0 t) + \frac{\dot{v}(0)}{\omega_0}\ \sin(\omega_0 t) + \\ &\sum_{k=1}^{N_{max}} C_k \cdot \cos((2k+1)\omega_0 t) + B_k \cdot \sin((2k+1)\omega_0 t)\ ,\end{aligned} \tag{32}$$

where the unknown parameters $C_i, B_i, i = 1, 2, 3, \cdots$, are optimally identified. This represents an approximate OHAM solution of Equation (5).

5. Numerical Results and Discussions

In this section, we discuss the accuracy of this method by taking into consideration the first-order approximate solution given by Equation (32), where $N_{max} \in \{5, 10, 20, 25\}$.

By means of Equations (3), (4) and (32), the approximate closed-form solutions of the Maxwell–Bloch equations are well-determined via the OHAM technique.

The accuracy of the obtained results is shown in Figures 1–4 and Tables A1 and A2 by comparison of the above-obtained approximate solutions with the corresponding numerical integration results, computed by means of the shooting method combined with the fourth-order Runge–Kutta method using Wolfram Mathematica 9.0 software. The convergence-control parameters $C_i, B_i, i = 1, 2, 3, \cdots N_{max}$, which appear in Equation (32), are computed by the least square method for different values of the known parameter N_{max}. From these figures, we can notice that there is symmetry with respect to the Oz-axis, and the periodicity is noticeable, which justified the choice of the time-limited value. Figure 5 highlights the symmetry of the 3D trajectory.

In Table A3, the values of the relative errors are presented, taking into account the index number N_{max}. The better approximate analytical solution corresponds to the value $N_{max} = 25$. This value was chosen for the efficiency of the solution.

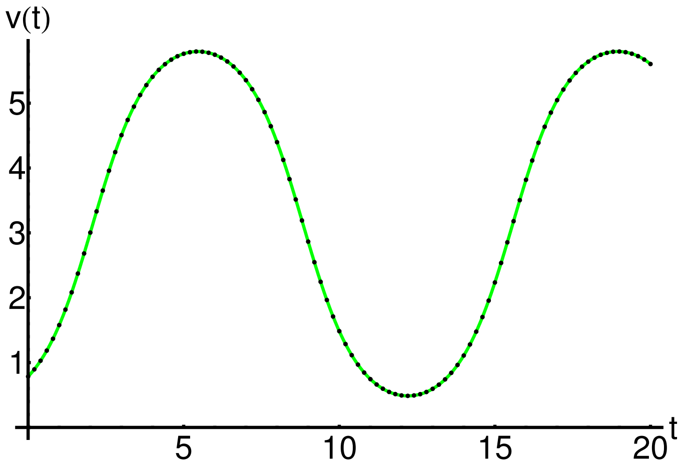

Figure 1. The auxiliary function $\bar{v}(t)$ given by Equation (32) using the initial conditions $x_0 = 0.5$, $y_0 = 0.5$, $z_0 = 0.5$ for $N_{max} = 25$: OHAM solution (with lines) and numerical solution (dashing lines), respectively.

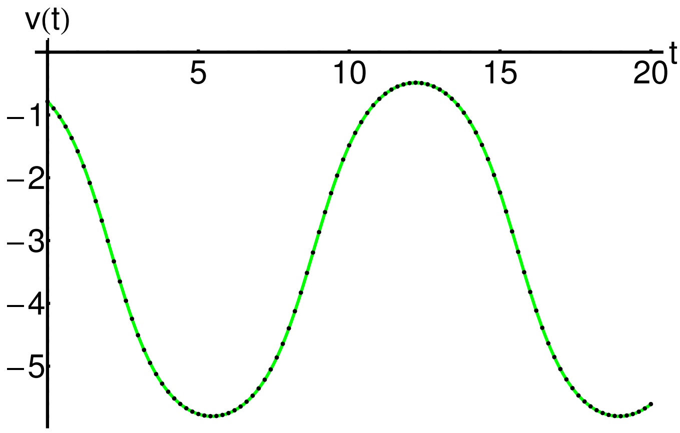

Figure 2. The auxiliary function $\bar{v}(t)$ given by Equation 32 using the initial conditions $x_0 = -0.5$, $y_0 = -0.5$, $z_0 = 0.5$ for $N_{max} = 25$: OHAM solution (with lines) and numerical solution (dashed lines), respectively.

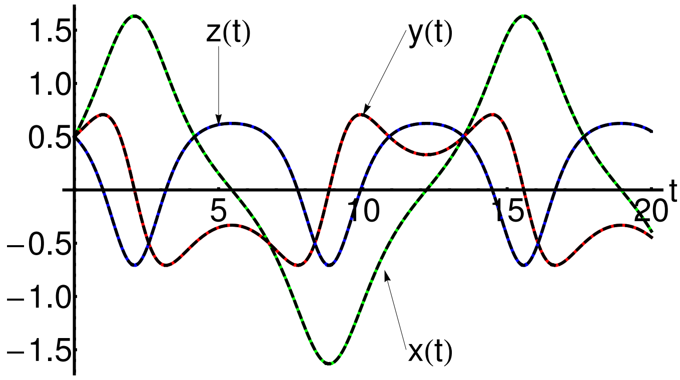

Figure 3. The set of solutions $x(t)$, $y(t)$, $z(t)$ given by Equations (3) and (4) using Equation (32) with the initial conditions $x_0 = 0.5$, $y_0 = 0.5$, $z_0 = 0.5$ for $N_{max} = 25$: OHAM solution (with lines) and numerical solution (dashed lines), respectively.

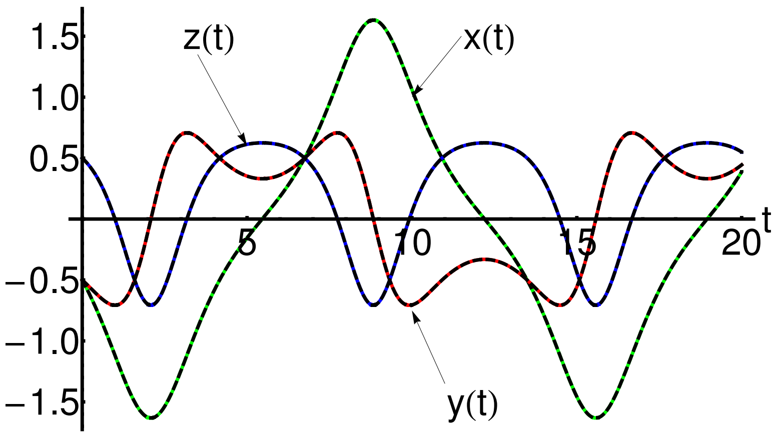

Figure 4. The set of solutions $x(t)$, $y(t)$, $z(t)$ given by Equations (3) and (4) using Equation (32) with the initial conditions $x_0 = -0.5$, $y_0 = -0.5$, $z_0 = 0.5$ for $N_{max} = 25$: OHAM solution (with lines) and numerical solution (dashed lines), respectively.

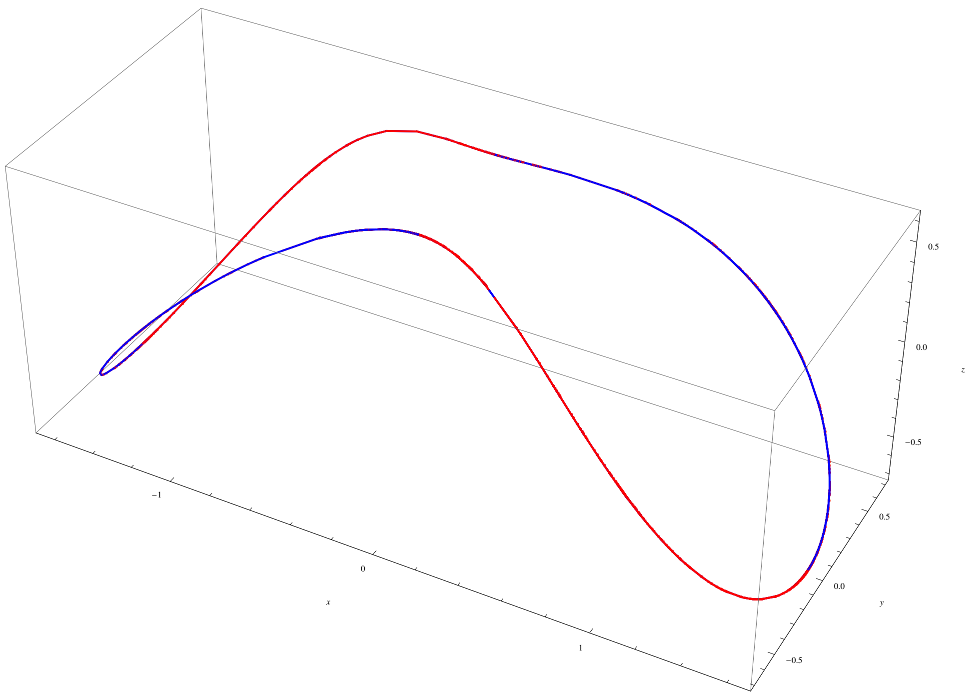

Figure 5. The parametric 3D curve $x = x(t)$, $y = y(t)$, $z = z(t)$ given by Equations (3) and (4) using Equation (32) with the initial conditions $x_0 = 0.5$, $y_0 = 0.5$, $z_0 = 0.5$ for $N_{max} = 25$: OHAM solution (with lines) and numerical solution (dashed lines), respectively.

6. Conclusions

In the present paper, some geometrical properties of the Maxwell–Bloch equations are emphasized, and the ε-approximate OHAM solutions were established. These obtained OHAM solutions, by comparison with the corresponding numerical solutions, lead to a good agreement. Moreover, the accuracy of the obtained results is validated for symmetric solutions with respect to the Oz-axis. The efficiency of the method is characterized by suitable values of the parameter N_{max}. The advantage is to obtain accurate solutions useful in many applications of technological interest.

Author Contributions: Conceptualization, N.P.; Data curation, R.E., N.P., M.L. and L.D.; Formal analysis, N.P.; Investigation, M.L. and L.D.; Methodology, R.E.; Software, R.E.; Supervision, N.P.; Validation, R.E., N.P. and L.D.; Visualization, R.E., N.P., M.L. and L.D.; Writing—original draft, R.E., N.P., M.L. and L.D. All authors have read and agreed to the published version of the manuscript.

Funding: This research received no external funding.

Institutional Review Board Statement: Not applicable.

Informed Consent Statement: Not applicable.

Data Availability Statement: Not applicable.

Conflicts of Interest: The authors declare no conflict of interest.

Appendix A

If the initial conditions are $x_0 = 0.5$, $y_0 = 0.5$ and $z_0 = 0.5$, for $N_{max} = 25$, then the approximate analytic solution $\bar{v}(t)$ given by Equation (32) becomes:

$$
\begin{aligned}
&\bar{v}(t) = \\
&= 0.7853981633 \cdot \cos(0.1212240932 \cdot t) + 1.1280863071 \cdot \cos(0.3636722796 \cdot t) - \\
&-0.3186517885 \cdot \cos(0.6061204660 \cdot t) - 0.1996129808 \cdot \cos(0.8485686525 \cdot t) - \\
&-0.2710466357 \cdot \cos(1.0910168389 \cdot t) - 0.3867642849 \cdot \cos(1.3334650253 \cdot t) - \\
&-0.1216474671 \cdot \cos(1.5759132118 \cdot t) - 0.0507600546 \cdot \cos(1.8183613982 \cdot t) + \\
&+0.0304281386 \cdot \cos(2.0608095846 \cdot t) + 0.0919966107 \cdot \cos(2.3032577711 \cdot t) + \\
&+0.0738209429 \cdot \cos(2.5457059575 \cdot t) + 0.0500084445 \cdot \cos(2.7881541439 \cdot t) + \\
&+0.0184363947 \cdot \cos(3.0306023304 \cdot t) - 0.0066048451 \cdot \cos(3.2730505168 \cdot t) - \\
&-0.0150894385 \cdot \cos(3.5154987033 \cdot t) - 0.0141512709 \cdot \cos(3.7579468897 \cdot t) - \\
&-0.0084535676 \cdot \cos(4.0003950761 \cdot t) - 0.0029454477 \cdot \cos(4.2428432626 \cdot t) + \\
&+0.0002250235 \cdot \cos(4.4852914490 \cdot t) + 0.0011645562 \cdot \cos(4.7277396354 \cdot t) + \\
&+0.0009265341 \cdot \cos(4.9701878219 \cdot t) + 0.0004806715 \cdot \cos(5.2126360083 \cdot t) + \\
&+0.0001433717 \cdot \cos(5.4550841947 \cdot t) + 0.0000179080 \cdot \cos(5.6975323812 \cdot t) - \\
&-1.648949 \cdot 10^{-6} \cdot \cos(5.9399805676 \cdot t) - 5.473392 \cdot 10^{-6} \cdot \cos(6.1824287540 \cdot t) + \\
&+4.1245926179 \cdot \sin(0.1212240932 \cdot t) + 2.7393061280 \cdot \sin(0.3636722796 \cdot t) - \\
&-1.1826779715 \cdot \sin(0.6061204660 \cdot t) - 0.4498691209 \cdot \sin(0.8485686525 \cdot t) - \\
&-0.2374141078 \cdot \sin(1.0910168389 \cdot t) - 0.1295416348 \cdot \sin(1.3334650253 \cdot t) + \\
&+0.1043902163 \cdot \sin(1.5759132118 \cdot t) + 0.1379494664 \cdot \sin(1.8183613982 \cdot t) + \\
&+0.1184346449 \cdot \sin(2.0608095846 \cdot t) + 0.0614542793 \cdot \sin(2.3032577711 \cdot t) + \\
&+0.0090494940 \cdot \sin(2.5457059575 \cdot t) - 0.0275951341 \cdot \sin(2.7881541439 \cdot t) - \\
&-0.0382993000 \cdot \sin(3.0306023304 \cdot t) - 0.0282586504 \cdot \sin(3.2730505168 \cdot t) - \\
&-0.0149834811 \cdot \sin(3.5154987033 \cdot t) - 0.0024357526 \cdot \sin(3.7579468897 \cdot t) + \\
&+0.0040036967 \cdot \sin(4.0003950761 \cdot t) + 0.0046957002 \cdot \sin(4.2428432626 \cdot t) + \\
&+0.0033601120 \cdot \sin(4.4852914490 \cdot t) + 0.0014744782 \cdot \sin(4.7277396354 \cdot t) + \\
&+0.0002834667 \cdot \sin(4.9701878219 \cdot t) - 0.0001047061 \cdot \sin(5.2126360083 \cdot t) - \\
&-0.0001492280 \cdot \sin(5.4550841947 \cdot t) - 0.0000740989 \cdot \sin(5.6975323812 \cdot t) - \\
&-0.0000204246 \cdot \sin(5.9399805676 \cdot t) - 3.372839 \cdot 10^{-6} \cdot \sin(6.1824287540 \cdot t)
\end{aligned}
\tag{A1}
$$

Table A1. Comparison between the obtained solutions $\bar{v}$ given by Equation (32) and numerical results for $x_0 = 0.5$, $y_0 = 0.5$ and $z_0 = 0.5$ (relative errors: $\epsilon_v = |v_{numerical} - \bar{v}_{OHAM}|$).

t	$v_{numerical}$	$\bar{v}_{OHAM}$	ϵ_v
0	0.7853981633	0.7853981633	1.110223×10^{-16}
2	3.0048565944	3.0048564682	1.262252×10^{-7}
4	5.4067162901	5.4067161112	1.789394×10^{-7}
6	5.7469951320	5.7469952686	1.366081×10^{-7}
8	4.3979496840	4.3979506058	9.217917×10^{-7}
10	1.4842095296	1.4842108567	1.327083×10^{-6}
12	0.4935555769	0.4935555528	2.405788×10^{-8}
14	1.1089381894	1.1089371304	1.058989×10^{-6}
16	3.8183645538	3.8183641247	4.291169×10^{-7}
18	5.6402614592	5.6402619962	5.369389×10^{-7}
20	5.6036661551	5.6036657121	4.429515×10^{-7}

Table A2. Comparison between the obtained solutions $\bar{v}$ given by Equation (32) and numerical results for $x_0 = -0.5$, $y_0 = -0.5$ and $z_0 = 0.5$ (relative errors: $\epsilon_\omega = |v_{numerical} - \bar{v}_{OHAM}|$).

t	$v_{numerical}$	$\bar{v}_{OHAM}$	ϵ_v
0	−0.7853981633	−0.7853981633	1.110223×10^{-16}
2	−3.0048565944	−3.0048564684	1.260096×10^{-7}
4	−5.4067162901	−5.4067161110	1.790516×10^{-7}
6	−5.7469951320	−5.7469952684	1.364679×10^{-7}
8	−4.3979496840	−4.3979506057	9.216750×10^{-7}
10	−1.4842095296	−1.4842108566	1.326997×10^{-6}
12	−0.4935555769	−0.4935555528	2.408859×10^{-8}
14	−1.1089381894	−1.1089371304	1.058966×10^{-6}
16	−3.8183645538	−3.8183641248	4.290359×10^{-7}
18	−5.6402614592	−5.6402619963	5.370392×10^{-7}
20	−5.6036661551	−5.6036657119	4.431479×10^{-7}

Table A3. Values of the relative errors $\epsilon_v = |v_{numerical} - \bar{v}_{OHAM}|$ for $x_0 = 0.5$, $y_0 = 0.5$, $z_0 = 0.5$ and different values of the index number N_{max}.

t	$N_{max} = 5$	$N_{max} = 10$	$N_{max} = 20$	$N_{max} = 25$
0	1.110223×10^{-16}	8.881784×10^{-16}	2.220446×10^{-16}	1.110223×10^{-16}
1/5	0.0057507451	0.0030455771	8.383820×10^{-4}	1.313631×10^{-6}
2/5	0.0227924915	0.0070594242	8.097412×10^{-4}	1.229725×10^{-6}
3/5	0.0494597939	0.0081429073	6.156841×10^{-5}	3.482073×10^{-7}
4/5	0.0825167222	0.0060042509	4.729830×10^{-4}	6.687728×10^{-7}
1	0.1176107773	0.0021559238	1.174198×10^{-4}	5.808890×10^{-7}
6/5	0.1499196854	0.0015691002	4.301057×10^{-4}	3.152192×10^{-7}
7/5	0.1749400518	0.0039327661	6.220876×10^{-4}	4.754099×10^{-7}
8/5	0.1892996460	0.0045783745	4.222215×10^{-4}	1.913513×10^{-7}
9/5	0.1914052506	0.0038272807	1.319308×10^{-4}	2.917863×10^{-7}
2	0.1817135046	0.0022665042	5.933946×10^{-6}	1.262252×10^{-7}

References

1. Lazureanu, C.; Caplescu, C. Stabilization of the T system by an integrable deformation. In *ITM Web of Conferences*; Third ICAMNM 2020; EDP Sciences: Les Ulis, France, 2020; Volume 34, p. 03009. [CrossRef]
2. Braga, D.C.; Dias, F.S.; Mello, L.F. On the stability of the equilibria of the Rikitake system. *Phys. Lett. A* **2010**, *374*, 4316–4320. [CrossRef]
3. Rikitake T. Oscillations of a system of disk dynamos. *Proc. Camb. Philos. Soc.* **1958**, *54*, 89–105. [CrossRef]

4. Steeb, W.H. Continuous symmetries of the Lorenz model and the Rikitake two-disc dynamo system. *J. Phys. A Math. Gen.* **1982**, *15*, 389–390. [CrossRef]
5. Binzar, T.; Lazureanu, C. On the symmetries of a Rabinovich type system. *Sci. Bull. Math. Phys.* **2012**, *57*, 29–36.
6. Lazureanu, C.; Binzar, T. Symmetries of some classes of dynamical systems. *J. Nonlinear Math. Phys.* **2015**, *22*, 265–274. [CrossRef]
7. Lazureanu, C.; Petrisor, C.; Hedrea, C. On a deformed version of the two-disk dynamo system. *Appl. Math.* **2021**, *66*, 345–372. [CrossRef]
8. Lazureanu, C.; Petrisor, C. Stability and energy-Casimir Mapping for integrable deformations of the Kermack-McKendrick system. *Adv. Math. Phys.* **2018**, *2018*, 5398768. [CrossRef]
9. Lazureanu, C. Integrable deformations of three-dimensional chaotic systems. *Int. J. Bifurcat. Chaos* **2018**, *28*, 1850066. [CrossRef]
10. Lazureanu, C. Hamilton-Poisson realizations of the integrable deformations of the Rikitake system. *Adv. Math. Phys.* **2017**, *2017*, 4596951. [CrossRef]
11. Lazureanu, C. The real-valued Maxwell-Bloch equations with controls: from a Hamilton-Poisson system to a chaotic one. *Int. J. Bifurcat. Chaos* **2017**, *27*, 1750143. [CrossRef]
12. Lazureanu, C. On a Hamilton-Poisson approach of the Maxwell-Bloch equations with a control. *Math. Phys. Anal. Geom.* **2017**, *20*, 20. [CrossRef]
13. Lazureanu, C.; Binzar, T. Symmetries and properties of the energy-Casimir mapping in the ball-plate problem. *Adv. Math.* **2017**, *2017*, 5164602. [CrossRef]
14. Lazureanu, C.; Binzar, T. On some properties and symmetries of the 5-dimensional Lorenz system. *Math. Probl. Eng.* **2015**, *2015*, 438694. [CrossRef]
15. Lazureanu, C.; Binzar, T. Some symmetries of a Rossler type system. *Sci. Bull. Math. Phys.* **2013**, *58*, 1–6.
16. Binzar, T.; Lazureanu, C. A Rikitake type system with one control. *Discrete Contin. Dyn. B* **2013**, *18*, 1755–1776. [CrossRef]
17. Lazureanu, C.; Binzar, T. Symplectic realizations and symmetries of a Lotka-Volterra type system. *Regul. Chaotic Dyn.* **2013**, *18*, 203–213. [CrossRef]
18. Lazureanu, C.; Binzar, T. A Rikitake type system with quadratic control. *Int. J. Bifur. Chaos* **2012**, *22*, 1250274. [CrossRef]
19. Lazureanu, C.; Binzar, T. On the symmetries of a Rikitake type system. *Comptes Rendus Math.* **2012**, *350*, 529–533. [CrossRef]
20. Lazureanu, C. On the Hamilton-Poisson realizations of the integrable deformations of the Maxwell-Bloch equations. *C. R. Acad. Sci. Paris Ser. I* **2017**, *355*, 596–600. [CrossRef]
21. Candido Murilo, R.; Llibre, J.; Valls, C. New symmetric periodic solutions for the Maxwell-Bloch differential system. *Math. Phys. Anal. Geom.* **2019**, *22*, 16. [CrossRef]
22. David, D.; Holm, D. Multiple Lie–Poisson structures, reduction and geometric phases for the Maxwell–Bloch traveling wave equations. *J. Nonlinear Sci.* **1992**, *2*, 241–262. [CrossRef]
23. Puta, M. On the Maxwell–Bloch equations with one control. *Comptes Rendus Acad. Sci. Paris Serie I* **1994**, *318*, 679–683.
24. Puta, M. Three dimensional real valued Maxwell–Bloch equations with controls. *Rep. Math. Phys.* **1996**, *3*, 337–348. [CrossRef]
25. Arecchi, F.T. Chaos and generalized multistability in quantum optics. *Phys. Scr.* **1985**, *9*, 85–92. [CrossRef]
26. Casu, I.; Lazureanu, C. Stability and integrability aspects for the Maxwell-Bloch equations with the rotating wave approximation. *Regul. Chaotic Dyn.* **2017**, *22* , 109–121. [CrossRef]
27. Zuo, D.W. Modulation instability and breathers synchronization of the nonlinear Schrodinger Maxwell–Bloch equation. *Appl. Math. Lett.* **2018**, *79*, 182–186. [CrossRef]
28. Wang, L.; Wang, Z.Q.; Sun, W.R.; Shi, Y.Y.; Li, M.; Xu, M. Dynamics of Peregrine combs and Peregrine walls in an inhomogeneous Hirota and Maxwell–Bloch system. *Commun. Nonlinear Sci. Numer. Simul.* **2017**, *47*, 190–199. [CrossRef]
29. Wei, J.; Wang, X.; Geng, X. Periodic and rational solutions of the reduced Maxwell–Bloch equations. *Commun. Nonlinear Sci. Numer. Simul.* **2018**, *59*, 1–14. [CrossRef]
30. Binzar, T.; Lazureanu, C. On some dynamical and geometrical properties of the Maxwell–Bloch equations with a quadratic control. *J. Geom. Phys.* **2013**, *70*, 1–8. [CrossRef]
31. Puta, M. Integrability and geometric prequantization of the Maxwell-Bloch equations. *Bull. Sci. Math.* **1998**, *122*, 243–250. [CrossRef]
32. El-Rashidy, K.; Seadawy, Aly, R.; Saad, Althobaiti, Makhlou, M.M. Multiwave, Kinky breathers and multi-peak soliton solutions for the nonlinear Hirota dynamical system. *Results Phys.* **2020**, *19*, 103678. [CrossRef]
33. Amer, T.S.; Bek, M.A.; Hassan, S.S.; Elbendary, S. The stability analysis for the motion of a nonlinear damped vibrating dynamical system with three-degrees-of-freedom. *Results Phys.* **2021**, *28*, 104561. [CrossRef]
34. Marinca, V.; Herisanu, N. Nonlinear dynamic analysis of an electrical machine rotor-bearing system by the optimal homotopy perturbation method. *Comput. Math. Appl.* **2011**, *61*, 2019–2024. [CrossRef]
35. Marinca, V.; Ene, R.D.; Marinca, B. Optimal Homotopy Perturbation Method for nonlinear problems with applications. *Appl. Comp. Math.* **2022**, *21*, 123–136.
36. Bota, C.; Caruntu, B.; Tucu, D.; Lapadat, M.; Pasca, M.S. A Least Squares Differential Quadrature Method for a Class of Nonlinear Partial Differential Equations of Fractional Order. *Mathematics* **2020**, *8*, 1336. [CrossRef]
37. Caruntu, B.; Bota, C.; Lapadat, M.; Pasca, M.S. Polynomial Least Squares Method for Fractional Lane-Emden Equations. *Symmetry* **2019**, *11*, 479. [CrossRef]

38. Marinca, V.; Draganescu, G.E. Construction of approximate periodic solutions to a modified van der Pol oscillator. *Nonlinear Anal. Real World Appl.* **2010**, *11*, 4355–4362. [CrossRef]
39. Herisanu, N.; Marinca, V. Accurate analytical solutions to oscillators with discontinuities and fractional-power restoring force by means of the optimal homotopy asymptotic method. *Comput. Math. Appl.* **2010**, *60*, 1607–1615. [CrossRef]
40. Safdar, H.; Abdullah, S.; Sana, A.; Asad, U. An approximate analytical solution of the Allen-Cahn equation using homotopy perturbation method and homotopy analysis method. *Heliyon* **2019**, *5*, e03060.
41. Wang, X.; Xu, Q.; Atluri, S.N. Combination of the variational iteration method and numerical algorithms for nonlinear problems. *Appl. Math. Model.* **2020**, *79*, 243–259. [CrossRef]
42. Turkyilmazoglu, M. An optimal variational iteration method. *Appl. Math. Lett.* **2011**, *24*, 762–765. [CrossRef]
43. Han, C.; Wang, Y.-L. Numerical Solutions of Variable-Coefficient Fractional-in-Space KdV Equation with the Caputo Fractional Derivative. *Fractal Fract.* **2022**, *6*, 207. [CrossRef]
44. Li, Z.; Chen, Q.; Wang, Y.; Li, X. Solving Two-Sided Fractional Super-Diffusive Partial Differential Equations with Variable Coefficients in a Class of New Reproducing Kernel Spaces. *Fractal Fract.* **2022**, *6*, 492. [CrossRef]
45. Marinca, V.; Herisanu, N. *The Optimal Homotopy Asymptotic Method—Engineering Applications*; Springer: Berlin/Heidelberg, Germany, 2015.
46. Paşca, M.S.; Bundău, O.; Juratoni, A.; Căruntu, B. The Least Squares Homotopy Perturbation Method for Systems of Differential Equations with Application to a Blood Flow Model. *Mathematics* **2022**, *10*, 546. [CrossRef]